Understanding the Long-term Trend of Organic Aerosol and the Influences from Anthropogenic Emission and Regional Climate Change in China

Wenxin Zhang[1], Yaman Liu[1,2], Man Yue[1,2], Xinyi Dong[1,3,4], Minghuai Wang[1,4]

[1]School of Atmospheric Science, Nanjing University, Nanjing, 210023, China
[2]Zhejiang Institute of Meteorological Sciences, Hangzhou, 310008, China
[3]Frontiers Science Center for Critical Earth Material Cycling, Nanjing University
[4]Joint International Research Laboratory of Atmospheric and Earth System Sciences & Institute for Climate and Global Change Research, Nanjing University, Nanjing, 210023, China

Correspondence to: Xinyi Dong (dongxy@nju.edu.cn)

Text S1: Model evaluation supplement. In addition to evaluating OA and its sub-species, this study also assessed other relevant factors that play a critical role in understanding the processes driving OA formation and its atmospheric impacts. O_3 was closely related to production of SOA as it was involved in VOCs-related chemistry. The model generally underestimated O_3 with a NMB of -17.9% compared to ground-based observations (Fig.S6(b)). Furthermore, since one of the pathways for the formation of SOA_{MT} involves reactions with the oxidant NO_2, we evaluated the model's simulation of NO_2 column density compared to satellite data, finding an NMB of 6.2% (Fig.S6(d)). In addition, as AOD is a crucial indicator of the total column burden of aerosols and plays an important role in understanding aerosol radiative effects, we also assessed the model's performance in simulating AOD (Fig.S6(c)), with an NMB of -41.4%. The model was found to be able to generally reproduce spatial distributions of these variables as well, with more details provided in Fig.S6. Simulation performance of CAM-Chem for O_3, NO_2 column density and AOD has been thoroughly discussed in recent publications (Emmons et al., 2020; Jo et al., 2021; Schwantes et al., 2020), and our results are in good agreement with these previous findings.

Text S2: Trend and attribution of Surface OA supplement. The annual variations of surface OA are presented by shaded areas representing contributions from POA and SOA as shown in Fig.S7(a). We find in the simulation that surface OA concentration increased by 5.6% (0.25 μg m^{-3}) over 1990-2019 as a combined result of a decrease in POA by -0.24 μg m^{-3} (-8.1%) and an increase in SOA by 0.49 μg m^{-3} (32.3%). Over the study period, proportion of POA in total OA decreased from 69.4% to 59.1% as shown in Fig.S7(a). It should be noticed that the change in OA was non-monotonical over the whole study period. Total OA concentration gradually increased by 1.7% per year over 1990-2006 and decreased by -3.2% per year over 2007-2019. Fig.S7(a) implies that neither changes in POA or SOA were monotonical, which was closely related to the implementation of anthropogenic emission management policies in China. In addition, changes of OA and subspecies at different seasons (Fig.S10) suggested that annual variation in OA was mainly driven by POA, which varied greatly in spring

and summer due to contributions from biomass burning (Fig.S11). More detailed discussions of the non-monotonical change and inter-annual variation will be provided in later subsections.

Text S3: In CAM6-Chem, SVOC emissions are determined by adding an additional 60% to the POM emissions, while IVOC emissions are calculated by adding an extra 20% to the non-methane VOC emissions (Tilmes et al., 2019). As shown in the formula below.

$$\mathrm{IVOC} = 0.2 * (\mathrm{C3H6} + \mathrm{C3H8} + \mathrm{C2H6} + \mathrm{C2H4} + \mathrm{BIGENE} + \mathrm{BIGALK} + \mathrm{CH3COCH3} + \mathrm{MEK} + \mathrm{CH3CHO} + \mathrm{CH2O} + \mathrm{BENZENE} + \mathrm{TOLUENE} + \mathrm{XYLENES}) \quad \text{(S1)}$$

$$\mathrm{SVOC} = 0.6 * \mathrm{pom\_a4} \quad \text{(S2)}$$

Species	Chemical formula	Description
C3H6	C_3H_6	propene
C3H8	C_3H_8	propane
C2H6	C_2H_6	ethane
C2H4	C_2H_4	ethene
BIGENE	C_4H_8	lumped alkenes C>3
BIGALK	C_5H_{12}	lumped alkanes C>3
CH3COCH3	CH_3COCH_3	acetone
MEK	C_4H_8O	methyl ethyl ketone
CH3CHO	CH_3CHO	acetaldehyde
CH2O	CH_2O	formaldehyde
BENZENE	C_6H_6	benzene
TOLUENE	C_7H_8	toluene
XYLENES	C_8H_{10}	lumped xylenes
pom_a4	C	primary organic matter, MAM primary carbon mode

Table S1. Species used for S/IVOC emission calculations.

year	SOA[1]	SOA[2]	POA[1]	POA[2]	OA[1]	OA[2]
1990	1.21	1.73	2.75	4.14	3.96	5.87

1991	1.22	1.73	2.75	4.14	3.98	5.87
1992	1.33	1.90	2.93	4.43	4.26	6.34
1993	1.21	1.72	2.72	4.09	3.94	5.80
1994	1.32	1.89	2.88	4.33	4.20	6.21
1995	1.26	1.79	2.85	4.27	4.11	6.06
1996	1.25	1.78	2.74	4.09	3.99	5.87
1997	1.38	1.97	2.94	4.39	4.32	6.36
1998	1.51	2.17	3.27	4.92	4.78	7.08
1999	1.26	1.78	2.75	4.08	4.01	5.85
2000	1.29	1.83	2.71	4.05	4.00	5.88
2001	1.31	1.87	2.76	4.12	4.07	5.99
2002	1.47	2.10	3.04	4.54	4.51	6.63
2003	1.77	2.58	3.90	5.89	5.67	8.47
2004	1.63	2.35	3.38	5.08	5.00	7.43
2005	1.56	2.24	3.19	4.79	4.75	7.03
2006	1.75	2.53	3.50	5.25	5.25	7.78
2007	1.80	2.62	3.48	5.25	5.28	7.87
2008	1.71	2.47	3.32	5.00	5.04	7.47
2009	1.77	2.54	3.31	4.93	5.07	7.48
2010	1.57	2.26	2.99	4.46	4.56	6.72
2011	1.73	2.52	3.23	4.85	4.96	7.37
2012	1.78	2.54	3.15	4.64	4.93	7.18

2013	1.86	2.72	3.19	4.77	5.05	7.49
2014	1.78	2.57	3.09	4.60	4.87	7.17
2015	1.70	2.45	2.76	4.10	4.46	6.55
2016	1.55	2.22	2.39	3.51	3.94	5.73
2017	1.45	2.07	2.23	3.28	3.68	5.35
2018	1.41	2.01	2.09	3.06	3.49	5.07
2019	1.49	2.13	2.14	3.16	3.63	5.29
multi-year arithmetic mean (ug/m^3)	1.51	2.17	2.95	4.41	4.46	6.58
Trend (ug/m^3 per year)	0.02	0.02	-0.01	-0.01	0.01	0.01
Trend (% per year)	1.08	1.12	-0.27	-0.32	0.19	0.15

Table S2. Simulated annual average concentrations (units: μg/m³) of surface OA, POA, and SOA from 1990 to 2019, along with their multi-year arithmetic mean (units: μg/m³) and trends. Superscript 1 indicates the calculation for the regional average concentration values for China, while superscript 2 indicates the calculation for the regional average concentration values for China excluding Xinjiang, Tibet, and Qinghai.

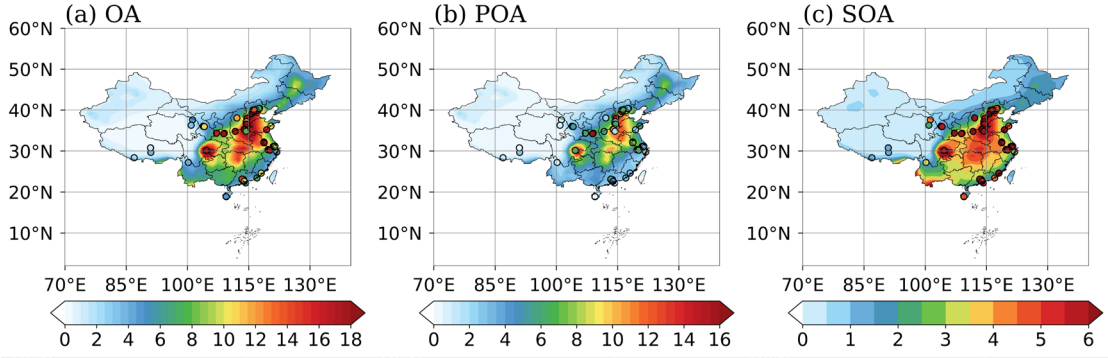

Figure S1. 2013 to 2019 annual average of surface organic aerosols (OA; a), primary organic aerosols (POA; b) and secondary organic aerosols (SOA; c) concentrations in our model and ground-based measurements (filled circles) compiled by Miao et al. (2021) and Chen et al. (2024) (unit: μg m^{-3}).

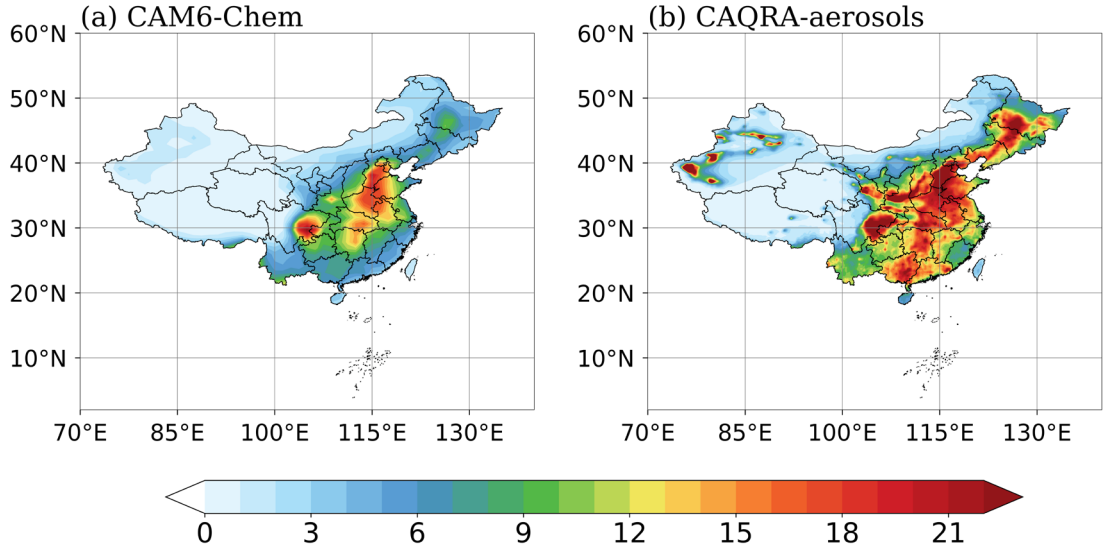

Figure S2. 2013 to 2019 annual average of surface organic aerosols (OA) concentrations in CAM6-Chem (a) and the CAQRA-aerosols dataset (b) (unit: μg m^{-3}).

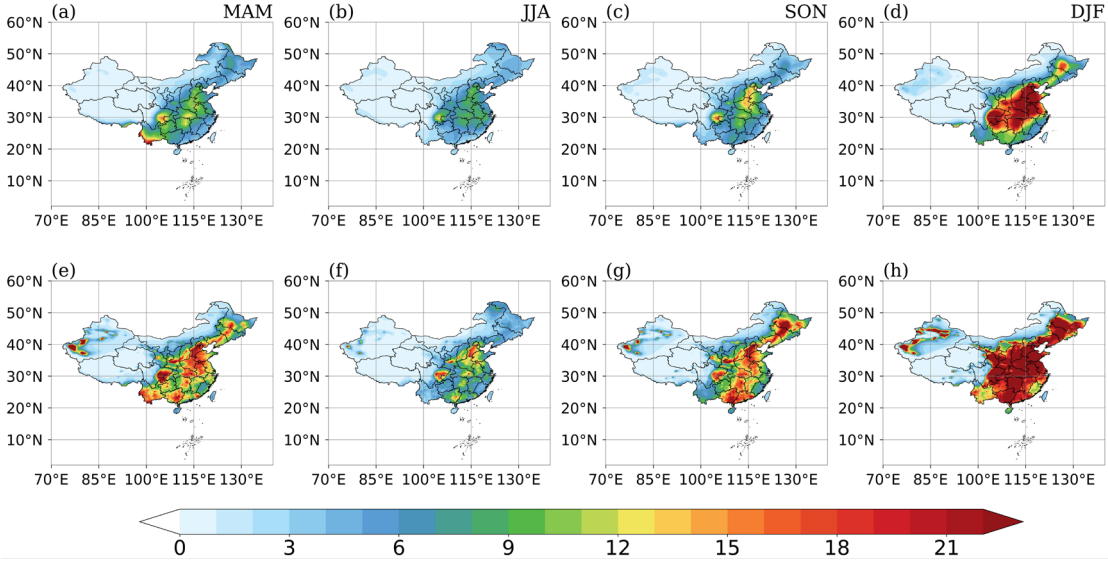

Figure S3. 2013 to 2019 MAM (first column), JJA (second column), SON (third column) and DJF (fourth column) average of surface organic aerosols (OA) concentrations in CAM6-Chem (first line) and the CAQRA-aerosols dataset (second line) (unit: μg m^{-3}).

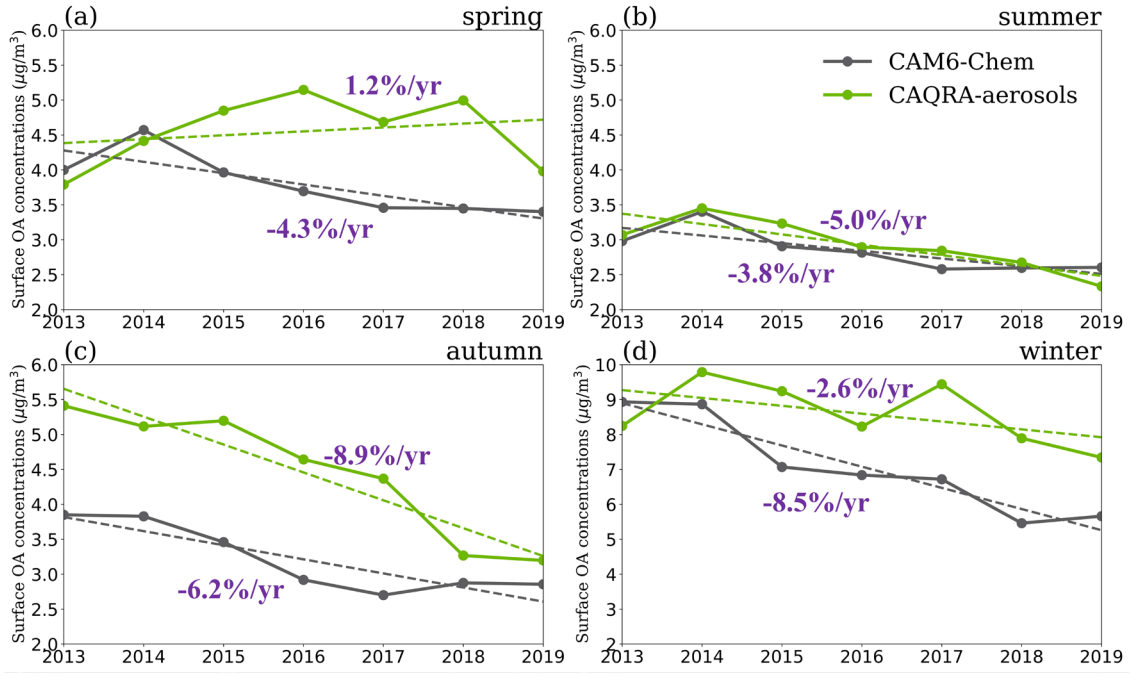

Figure S4. 2013 to 2019 interannual variation of different seasonal average surface organic aerosol (OA) concentrations in CAM6-Chem (dark grey) and the CAQRA-aerosols dataset (green) (unit: μg m^{-3}) and their trend lines (dotted line).

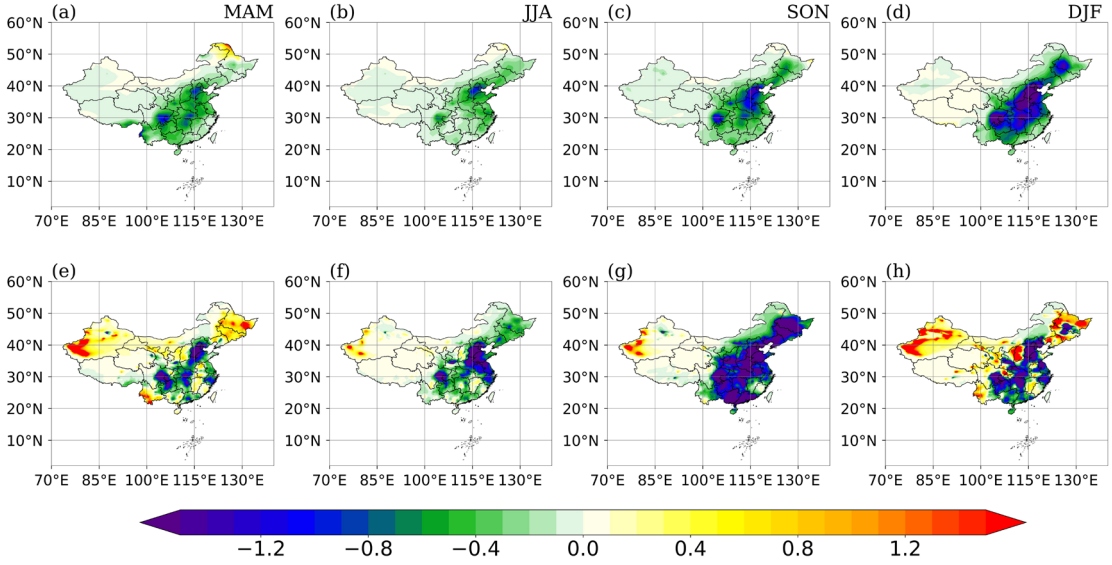

Figure S5. 2013 to 2019 MAM (first column), JJA (second column), SON (third column) and DJF (fourth column) average long-term trend of surface organic aerosols (OA) concentrations in CAM6-Chem (first line) and the CAQRA-aerosols dataset (second line) (unit: μg m^{-3} per year).

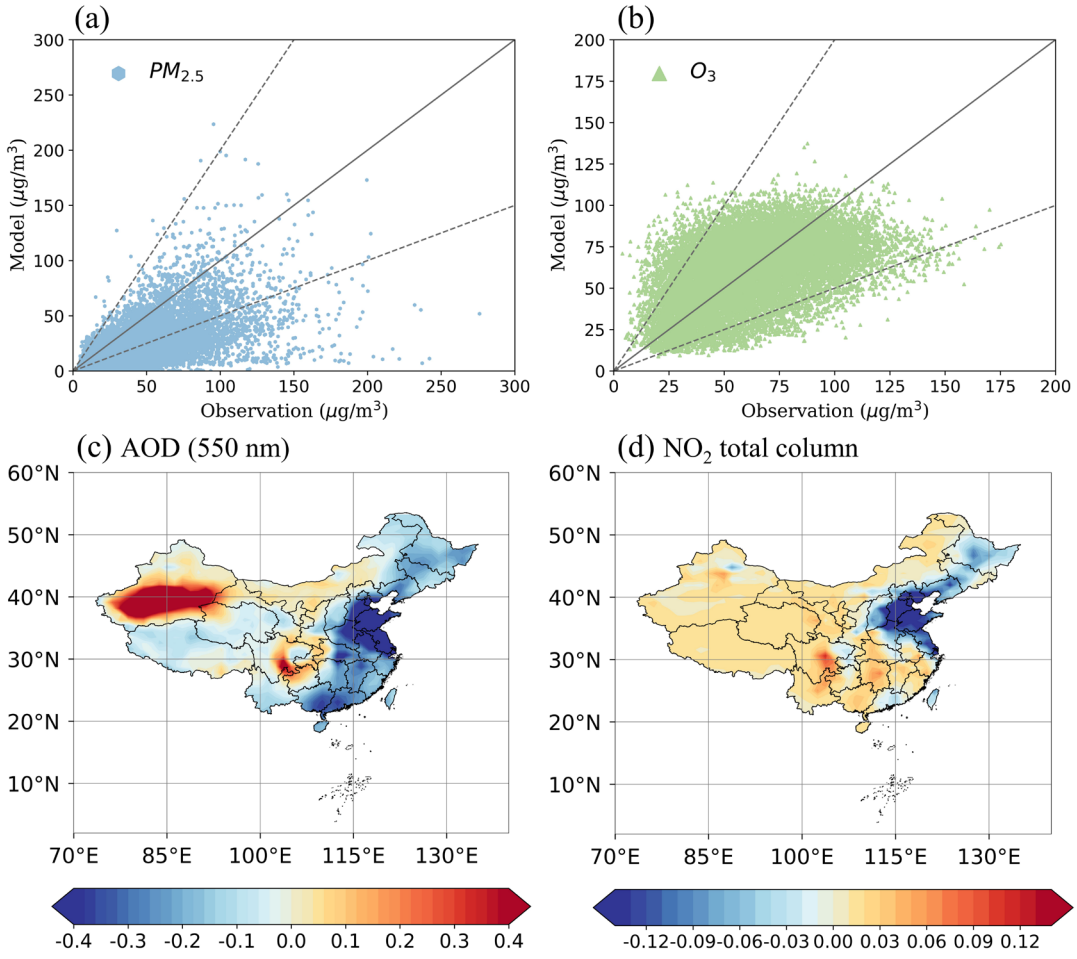

Figure S6. Validation of modelled surface $PM_{2.5}$ (a) and O_3 (b) concentrations based on the National Urban Air Quality Real-Time Dissemination Platform of the China Environmental Monitoring General Station (unit: μg m^{-3}) from 2014 to 2019. The annual average climatological difference between the aerosol optical depth (AOD) (c) and the NO_2 column concentrations (d; unit: Tg) simulated by the model and satellite observations from 2000 to 2019.

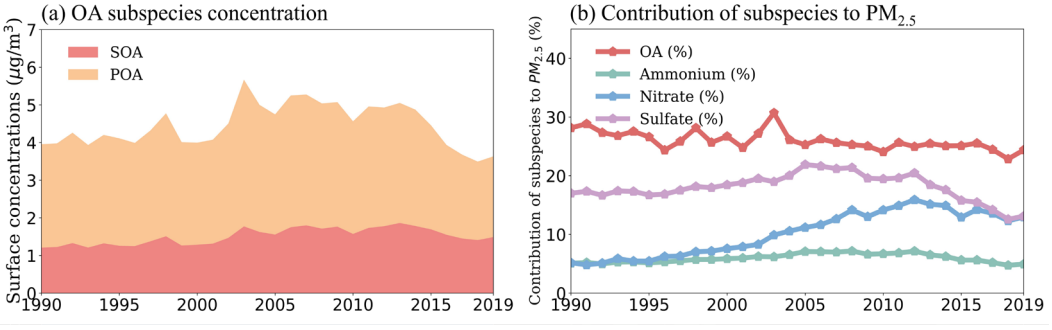

Figure S7. (a) Interannual variations in modelled surface concentrations of organic aerosols (OA) subspecies primary organic aerosols (POA) and secondary organic aerosols (SOA) (unit: μg m^{-3}). (b) Interannual variations in the proportion of important components (OA, sulfate, nitrate, and ammonium) of $PM_{2.5}$ (unit: %).

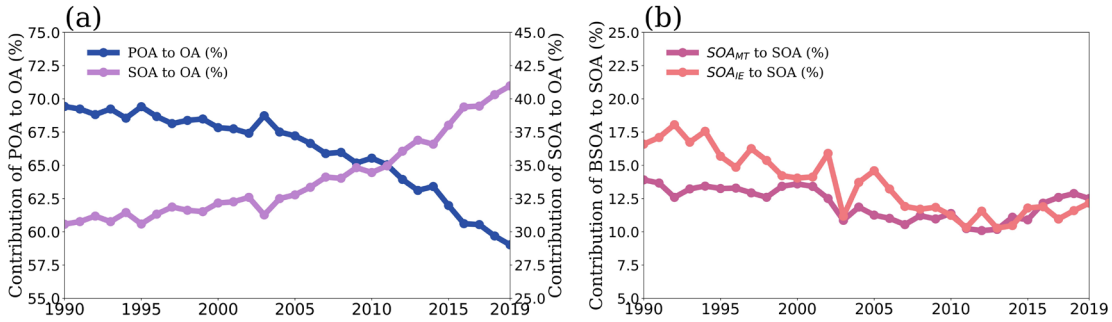

Figure S8. (a) Interannual variations in the contribution of subspecies primary organic aerosols (POA) and secondary organic aerosols (SOA) to organic aerosols (OA) (unit: %). (b) Interannual variations in the contribution of subspecies isoprene-epoxydiol-derived secondary organic aerosols (SOA_{IE}) and monoterpene-derived secondary organic aerosols (SOA_{MT}) to SOA (unit: %).

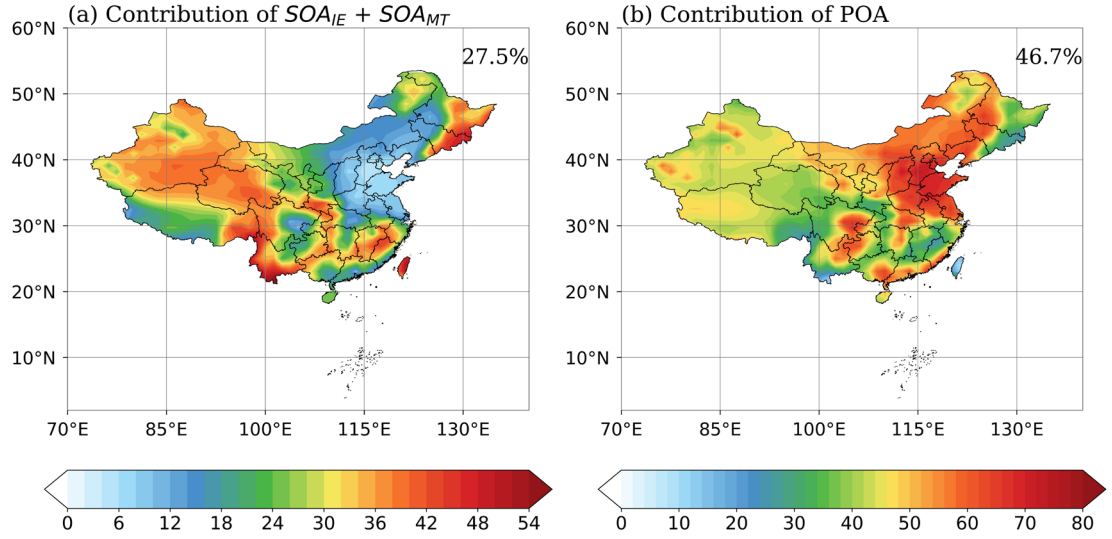

Figure S9. (a) 1990 to 2019 JJA average contribution of isoprene-epoxydiol-derived secondary organic aerosols + monoterpene-derived secondary organic aerosols (SOA_{IE} + SOA_{MT}) to organic aerosols (OA) (unit: %). (b) 1990 to 2019 JJA average contribution of primary organic aerosols (POA) to OA (unit: %). Spatial averages are shown in the upper right corner.

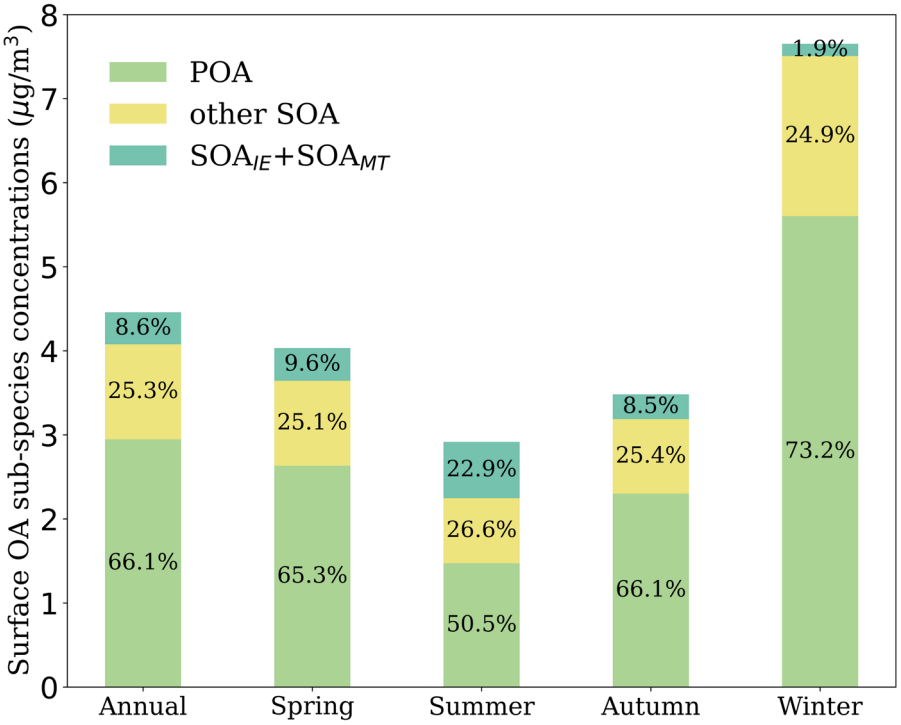

Figure S10. Annual and seasonal average contributions of organic aerosols (OA) subspecies primary organic aerosols (POA), isoprene-epoxydiol-derived secondary organic aerosols + monoterpene-derived secondary organic aerosols (SOA$_{IE}$ + SOA$_{MT}$) and other secondary organic aerosols (SOA) to OA.

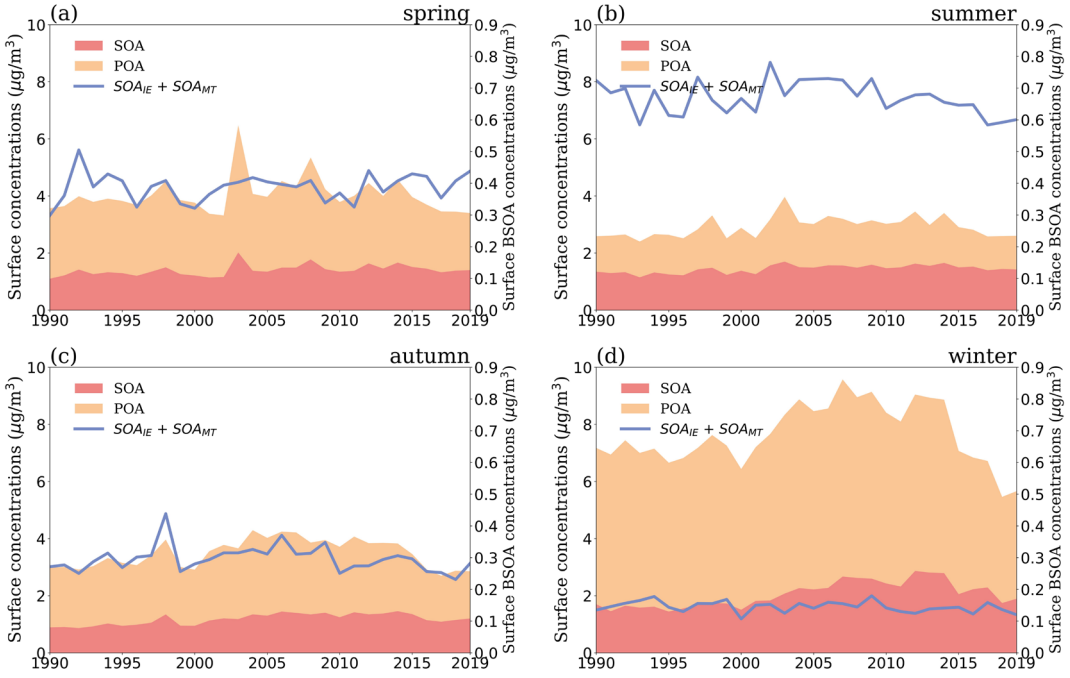

Figure S11. Seasonal average variation in modelled surface concentrations of organic aerosols (OA) subspecies primary organic aerosols (POA; left Y axis), secondary organic aerosols (SOA; left Y axis), isoprene-epoxydiol-derived secondary organic aerosols + monoterpene-derived secondary organic aerosols (SOA_{IE} + SOA_{MT}; right Y axis) (unit: μg m^{-3}).

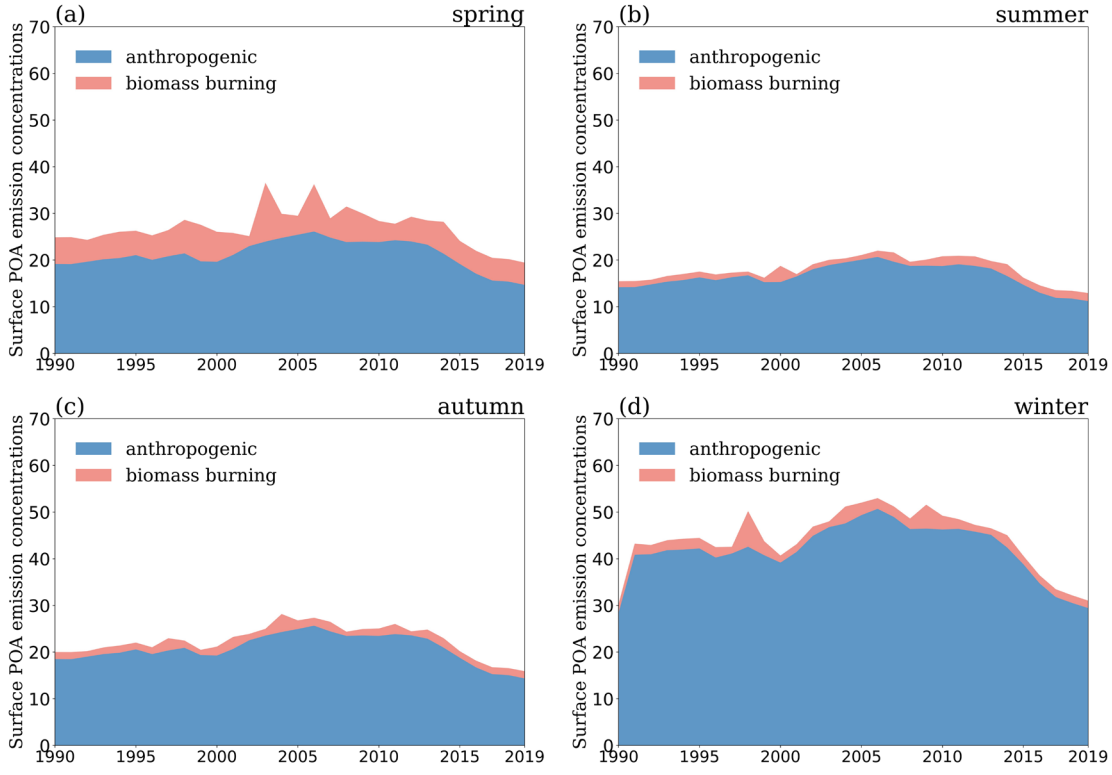

Figure S12. 1990 to 2019 seasonal average variation of surface anthropogenic (blue) and biomass burning (pink) primary organic aerosols (POA) emissions (unit: g m^{-2} mon^{-1}).

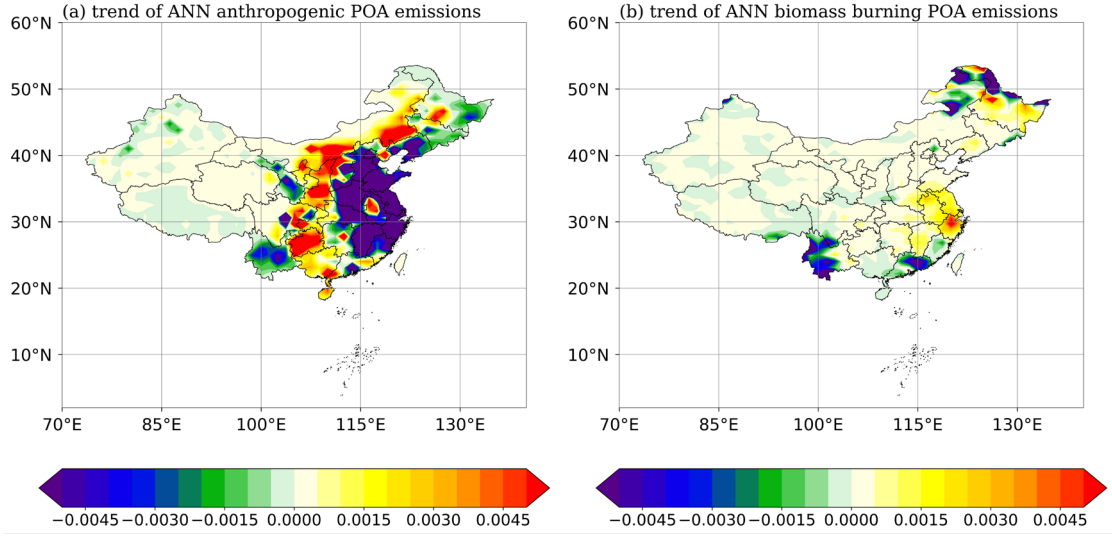

Figure S13. 1990 to 2019 annual average long-term trend of anthropogenic primary organic aerosols (POA) emissions (a; unit: g m^{-2} per decade) and biomass burning POA emissions (b; unit: g m^{-2} per decade).

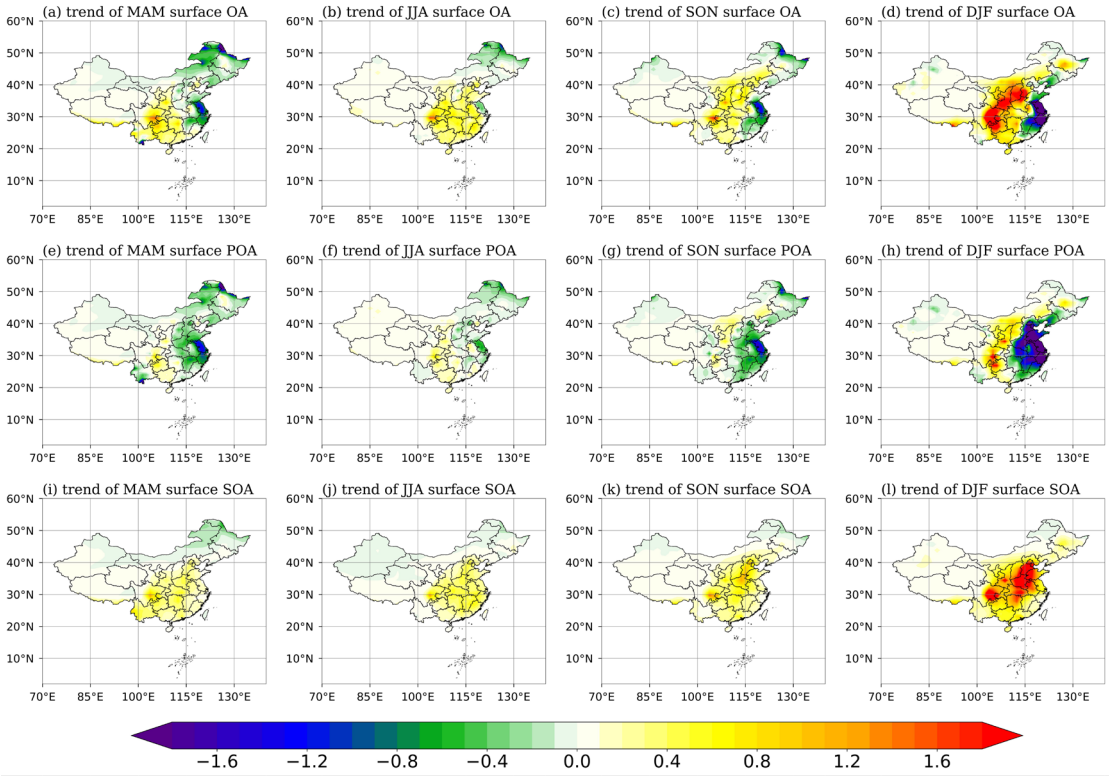

Figure S14. 1990 to 2019 MAM (first column), JJA (second column), SON (third column) and DJF (fourth column) average long-term trend of surface organic aerosols (OA; a-d) and its components primary organic aerosols (POA; e-h)、secondary organic aerosols (SOA; i-l) concentrations (unit: μg m^{-3} per decade).

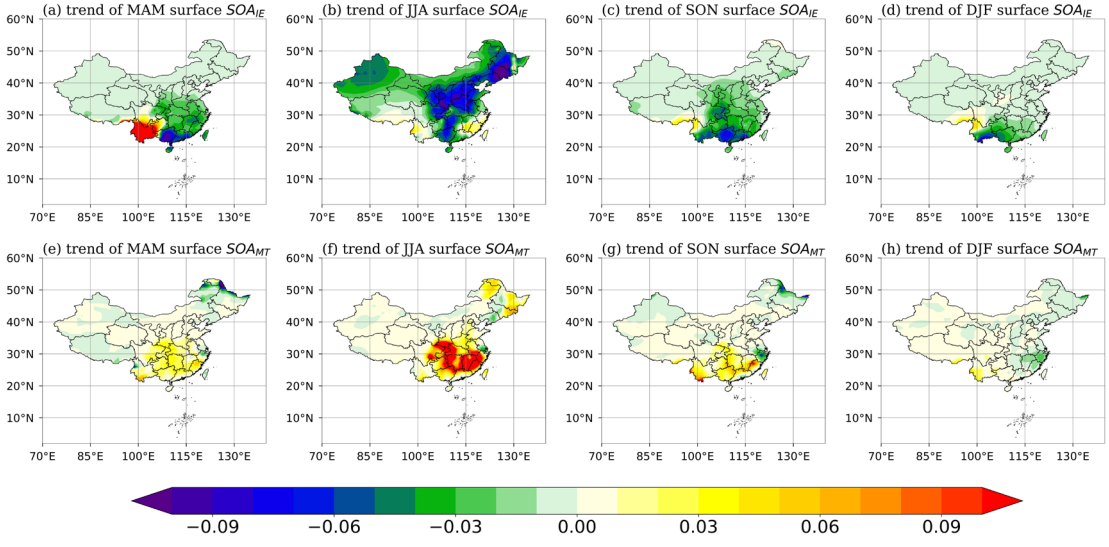

Figure S15. 1990 to 2019 MAM (first column), JJA (second column), SON (third column) and DJF (fourth column) average long-term trend of surface isoprene-epoxydiol-derived secondary organic aerosols (SOA_{IE}; a-d) and monoterpene-derived secondary organic aerosols (SOA_{MT}; e-h) concentrations (unit: μg m^{-3} per decade).

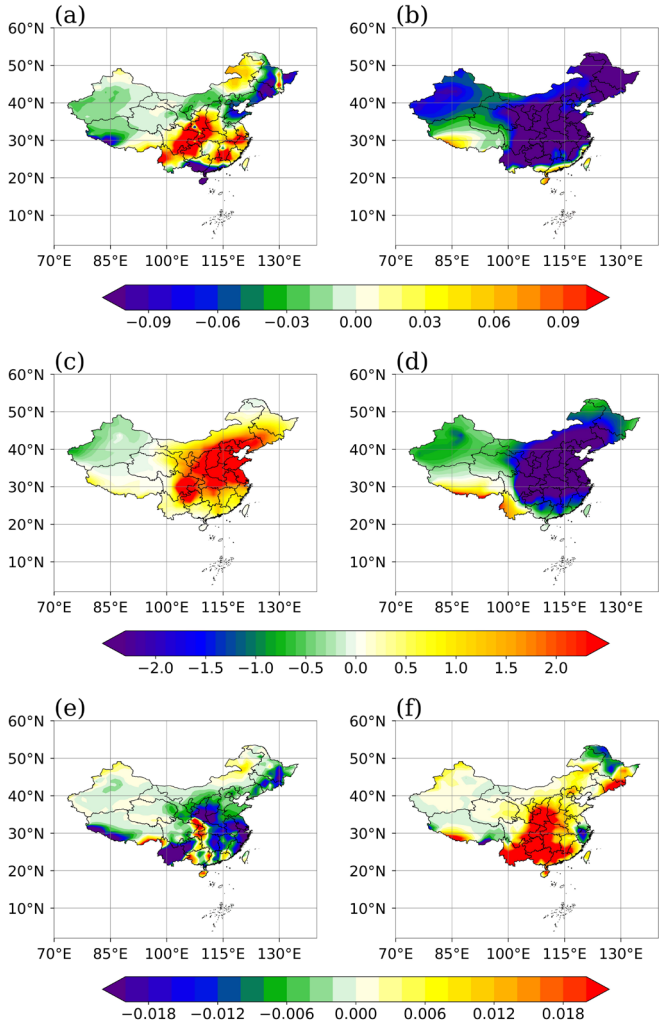

Figure S16. The JJA average long-term trends of surface isoprene-epoxydiol-derived secondary organic aerosols (SOA_{IE}; a-b; unit: μg m^{-3} per decade), organosulfate (SO_4^{2-}; c-d; unit: μg m^{-3} per decade), and isoprene epoxydiol (IEPOX; e-f; unit: ppb per decade) concentrations for the periods 1990-2006 (left column) and 2006-2019 (right column).

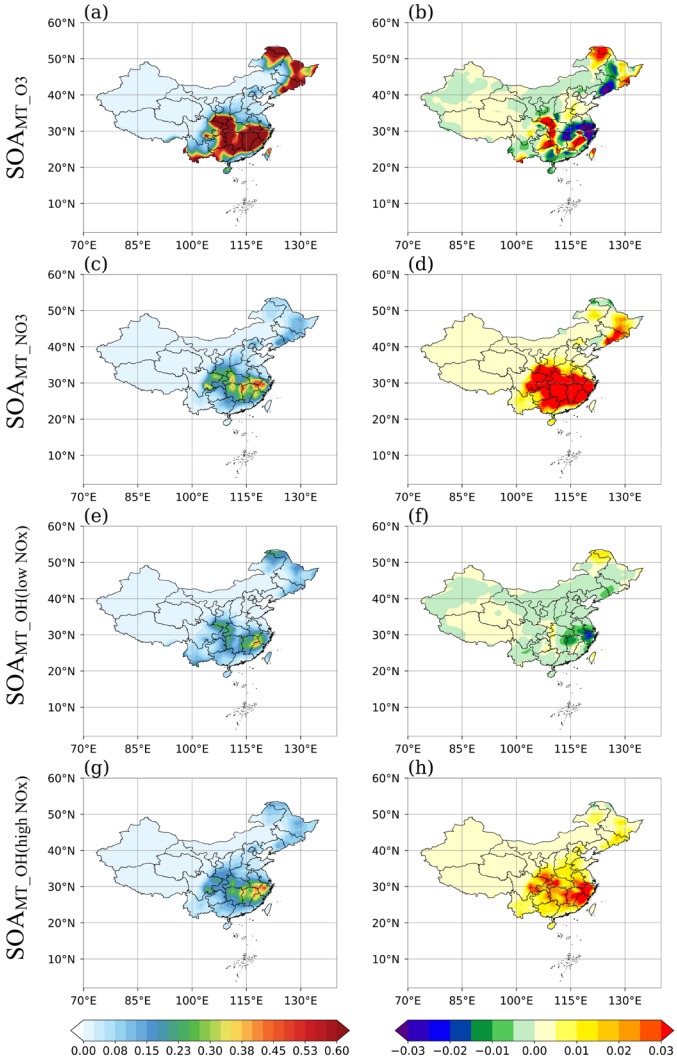

112 **Figure S17. 1990 to 2019 JJA average (left column; unit: μg m^{-3}) and long-term trend (right column; unit: μg m^{-3} per decade) of surface monoterpene-derived secondary organic aerosols (SOA_{MT}) oxidized by O_3 ($SOA_{MT\_O_3}$; a-b), SOA_{MT} oxidized by NO_3**
114 **($SOA_{MT\_NO_3}$; c-d), SOA_{MT} oxidized by OH under low NOx condition ($SOA_{MT\_OH(low\ NOx)}$; e-f) and SOA_{MT} oxidized by OH under high NOx condition ($SOA_{MT\_OH(high\ NOx)}$; g-h) concentrations.**

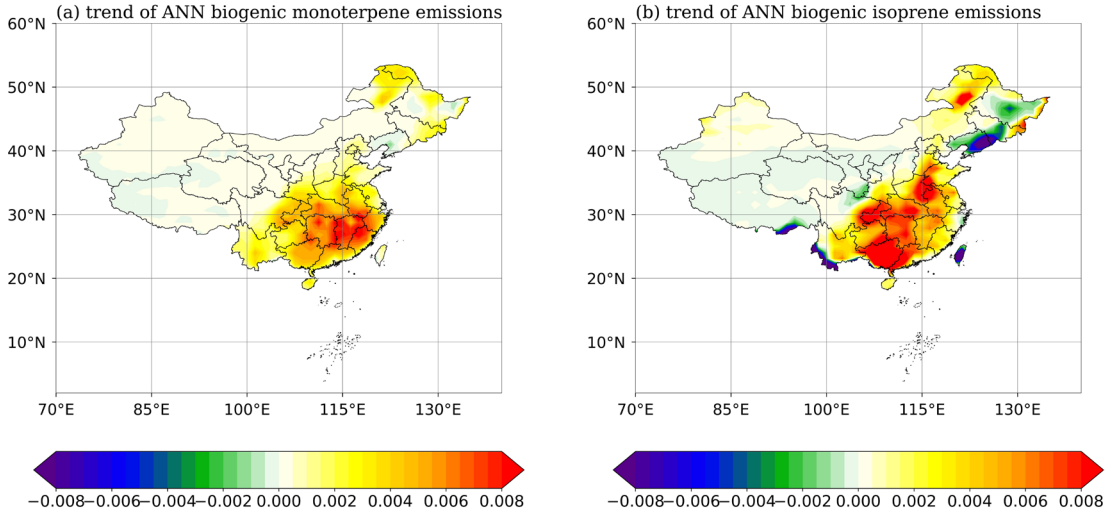

116

Figure S18. 1990 to 2019 annual average long-term trend of biogenic monoterpene emissions (a) and biogenic isoprene emissions (b)
118 **(unit: g m^{-2} per decade).**

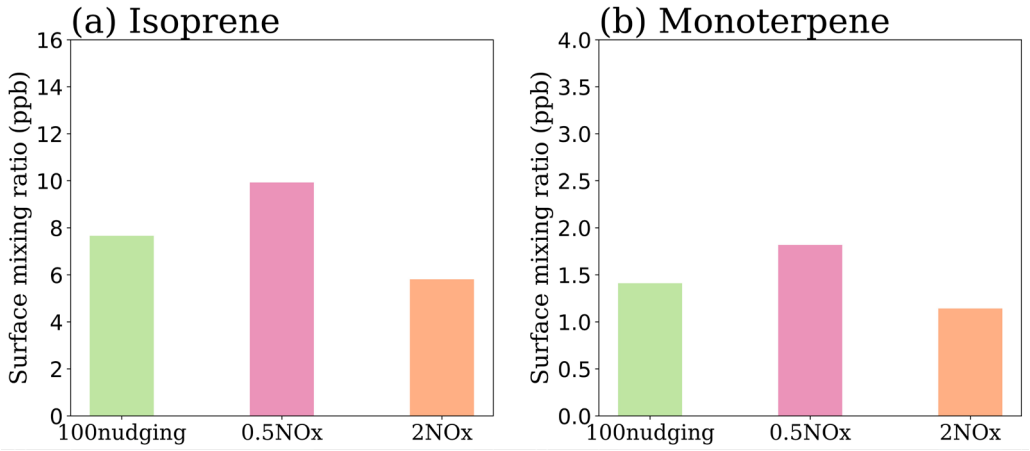

120 **Figure S19. Surface concentrations (unit: ppb) of (a) isoprene and (b) monoterpene for July 2013 from the NOx sensitivity experiments named 100nudging (green bar), 0.5NOx (pink bar) and 2NOx (orange bar).**

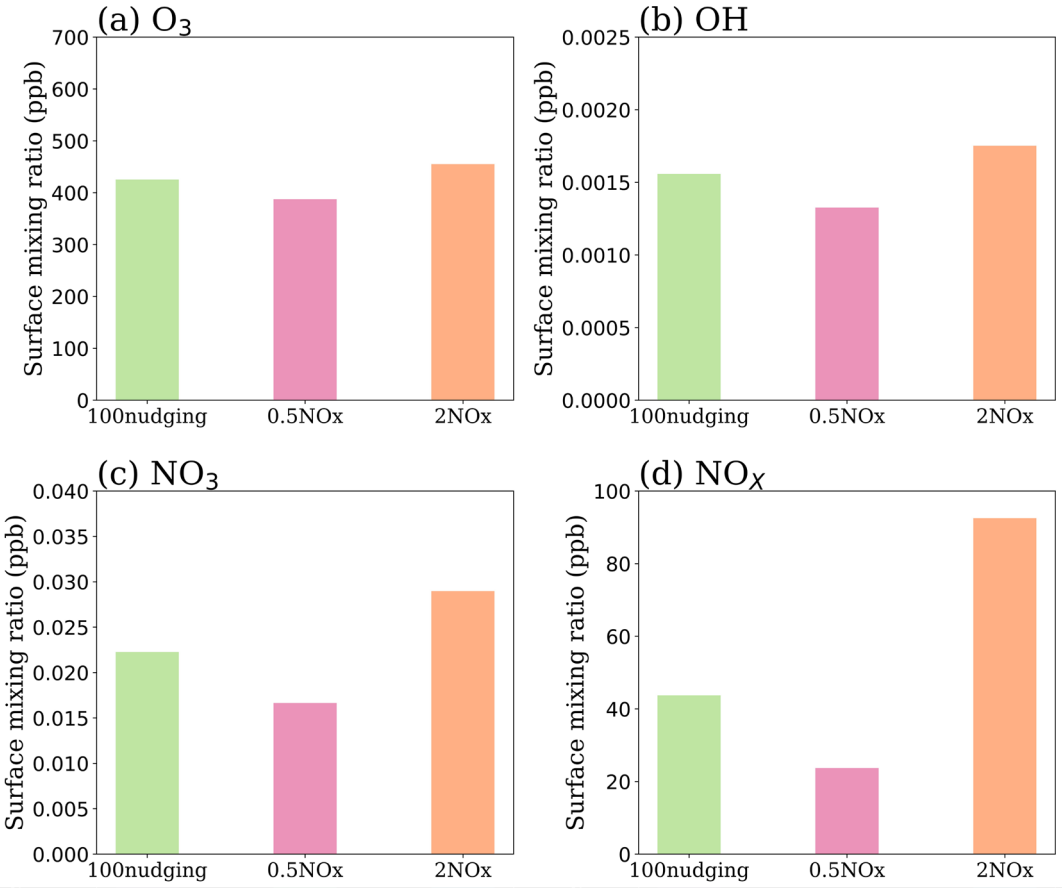

Figure S20. Surface concentrations (unit: ppb) of (a) O_3, (b) OH, (c) NO_3 and (d) NOx for July 2013 from the NOx sensitivity experiments named 100nudging (green bar), 0.5NOx (pink bar) and 2NOx (orange bar).

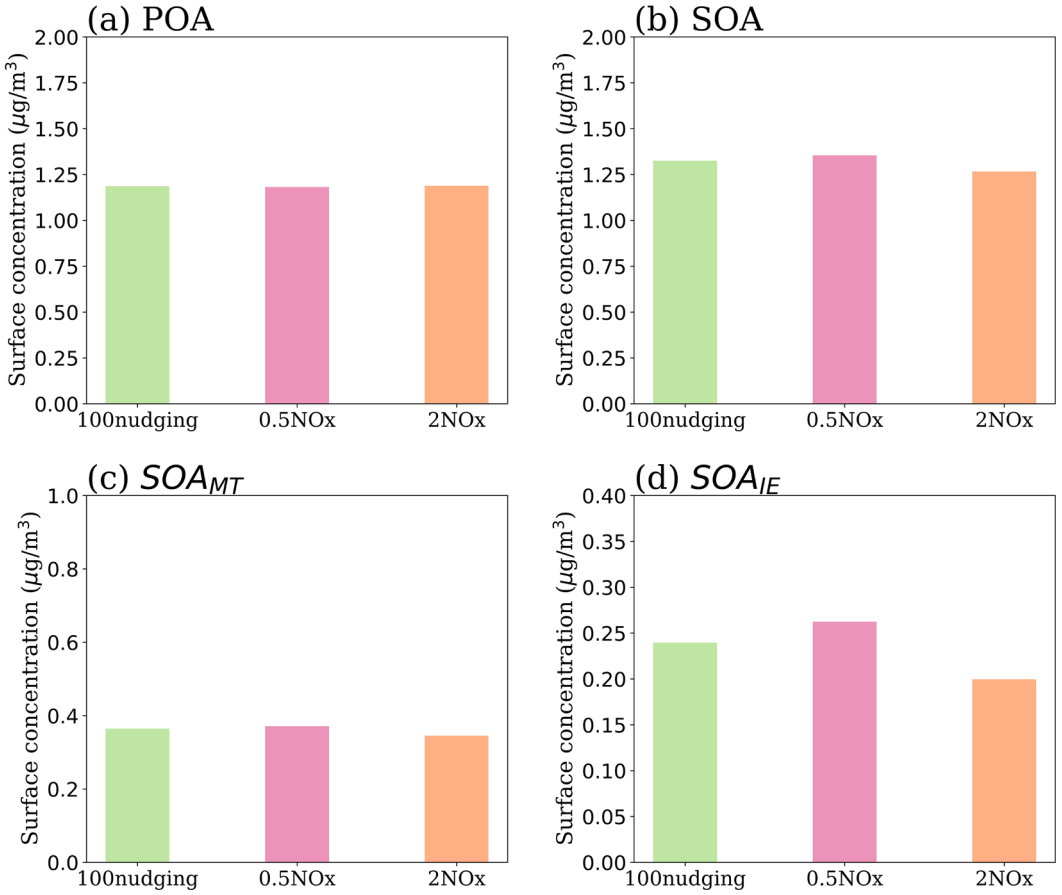

126 **Figure S21. Surface concentrations (unit: μg m^{-3}) of primary organic aerosols (POA; a), secondary organic aerosols (SOA; b), monoterpene-derived secondary organic aerosols (SOA_{MT}; c), isoprene-epoxydiol-derived secondary organic aerosols (SOA_{IE}; d) for**
128 **July 2013 from the NOx sensitivity experiments named 100nudging (green bar), 0.5NOx (pink bar) and 2NOx (orange bar).**

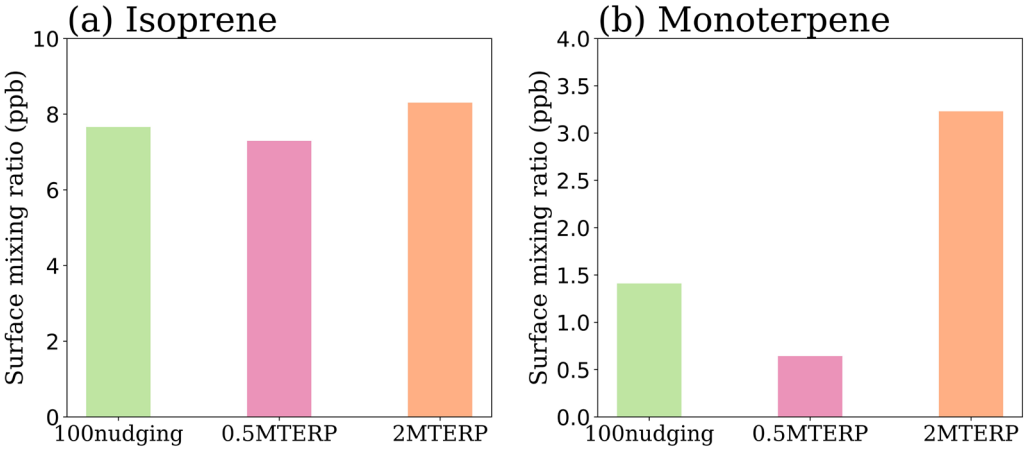

130

Figure S22. Surface concentrations (unit: ppb) of (a) isoprene and (b) monoterpene for July 2013 from the monoterpene sensitivity experiments named 100nudging (green bar), 0.5MTERP (pink bar), and 2MTERP (orange bar).

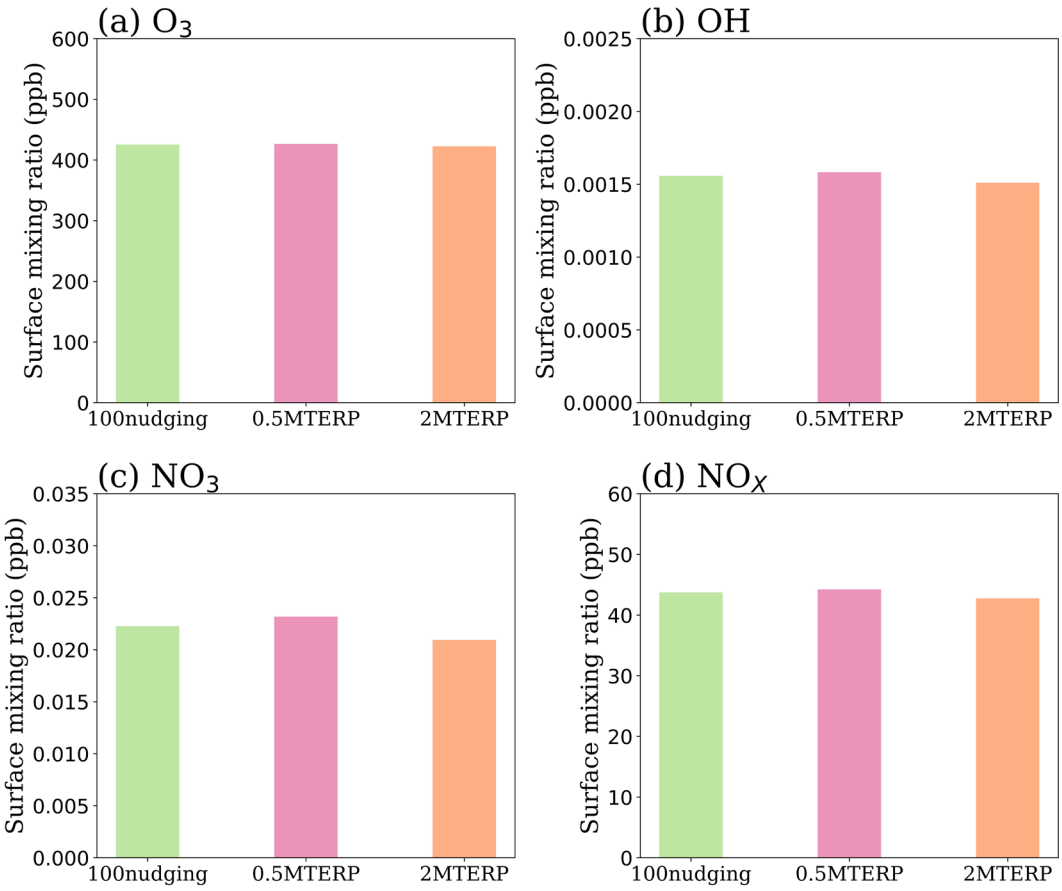

Figure S23. Surface concentrations (unit: ppb) of (a) O_3, (b) OH, (c) NO_3 and (d) NOx for July 2013 from the monoterpene sensitivity experiments named 100nudging (green bar), 0.5MTERP (pink bar), and 2MTERP (orange bar).

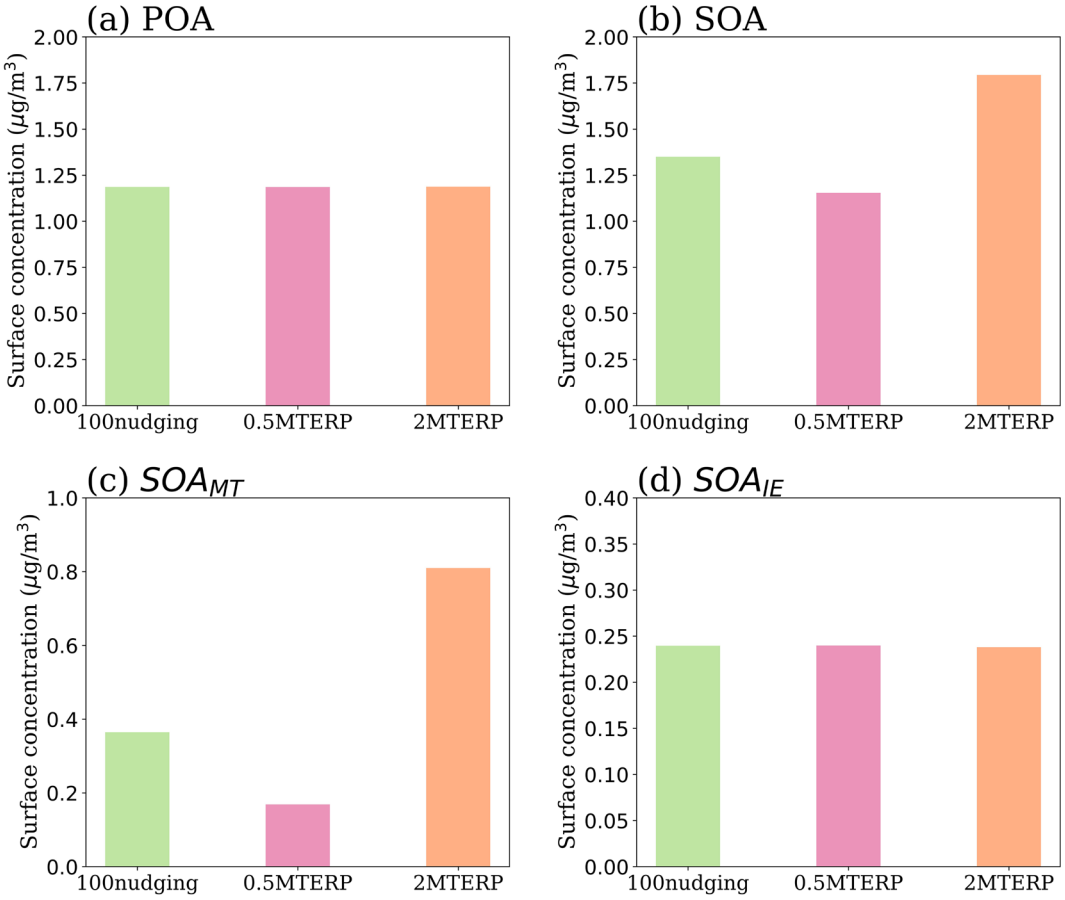

Figure S24. Surface concentrations (unit: μg m^{-3}) of primary organic aerosols (POA; a), secondary organic aerosols (SOA; b), monoterpene-derived secondary organic aerosols (SOA_{MT}; c), isoprene-epoxydiol-derived secondary organic aerosols (SOA_{IE}; d) for July 2013 from the monoterpene sensitivity experiments named 100nudging (green bar), 0.5MTERP (pink bar), and 2MTERP (orange bar).

References

Emmons, L. K., Schwantes, R. H., Orlando, J. J., Tyndall, G., Kinnison, D., Lamarque, J., Marsh, D., Mills, M. J., Tilmes, S., Bardeen, C., Buchholz, R. R., Conley, A., Gettelman, A., Garcia, R., Simpson, I., Blake, D. R., Meinardi, S., and Pétron, G.: The Chemistry Mechanism in the Community Earth System Model Version 2 (CESM2), J Adv Model Earth Syst, 12, e2019MS001882, https://doi.org/10.1029/2019MS001882, 2020.

Jo, D. S., Hodzic, A., Emmons, L. K., Tilmes, S., Schwantes, R. H., Mills, M. J., Campuzano-Jost, P., Hu, W., Zaveri, R. A., Easter, R. C., Singh, B., Lu, Z., Schulz, C., Schneider, J., Shilling, J. E., Wisthaler, A., and Jimenez, J. L.: Future changes in isoprene-epoxydiol-derived secondary organic aerosol (IEPOX SOA) under the Shared Socioeconomic Pathways: the

importance of physicochemical dependency, Atmos. Chem. Phys., 21, 3395–3425, https://doi.org/10.5194/acp-21-3395-2021, 2021.

Schwantes, R. H., Emmons, L. K., Orlando, J. J., Barth, M. C., Tyndall, G. S., Hall, S. R., Ullmann, K., St. Clair, J. M., Blake, D. R., Wisthaler, A., and Bui, T. P. V.: Comprehensive isoprene and terpene gas-phase chemistry improves simulated surface ozone in the southeastern US, Atmos. Chem. Phys., 20, 3739–3776, https://doi.org/10.5194/acp-20-3739-2020, 2020.

Tilmes, S., Hodzic, A., Emmons, L. K., Mills, M. J., Gettelman, A., Kinnison, D. E., Park, M., Lamarque, J. -F., Vitt, F., Shrivastava, M., Campuzano-Jost, P., Jimenez, J. L., and Liu, X.: Climate Forcing and Trends of Organic Aerosols in the Community Earth System Model (CESM2), J. Adv. Model. Earth Syst., 11, 4323–4351, https://doi.org/10.1029/2019MS001827, 2019.